MODELING, IDENTIFICATION AND CONTROL, 1981, VOL. 2, NO. 2, 57–70
doi: 10.4173/mic.1981.2.1

On ultrasonic MTI measurement of velocity profiles in blood flow†

BJØRN A. J. ANGELSEN‡§ and KJELL KRISTOFFERSEN‡

Keywords: *ultrasound, doppler effect, blood flow, velocity profiles.*

A theoretical analysis of Doppler frequency estimators proposed to be used in ultrasonic MTI measurements of velocity profiles in blood flow, is given. The estimators give an output in form of a single analogue voltage and the relation of the output to the Doppler spectrum is discussed. Three new estimators are also proposed. All estimators work fairly well for narrow-band Doppler spectra, but errors are found when broad-band spectra are present.

1. Introduction

The moving target indicator (MTI) (Skolnik 1962) is used for detecting weak radar echoes from moving objects in a background of strong clutter echoes from stationary targets. The basic principle is to compare the echoes from two following pulses and detect the change in the signal:

(i) By subtracting the echoes of one pulse from the echoes of the next, the echoes from stationary targets are removed. This method is called fixed target cancelling (FTC).

(ii) After the echoes from fixed targets have been removed, the phase change between the echoes of adjacent pulses can be compared, in order to determine the velocity of moving objects (Doppler effect).

More advanced FTCs than the one above can be constructed in order to reject signals from targets with velocity below a certain limit (comb filters) (Skolnik 1962).

Recently there has been some interest in applying this method for estimating velocity profiles in blood vessels by comparing the backscattered signal from ultrasonic pulses (Grandchamp 1975, Brandestini 1976, 1977). Although the basic principle is simple and appealing, it requires storage of the echoes, which complicates its experimental application. In biological measurements the scattered signal from blood can be as much as 60 dB below the signal scattered from slowly moving tissue. Therefore a higher order comb filter is necessary for FTC, which requires storage of the echoes from several pulses. The FTC problem is, however, not considered here.

The simplest Doppler frequency estimator is a phase comparison between the echoes from adjacent pulses. This works well when a single Doppler frequency is present. In blood velocity measurements the scatterers are distributed in space with a space dependent velocity field. Owing to the limited space resolution (minimum

Received 6 May, 1980.

† This paper has been published in *I.E.E.E. Transactions on Biomedical Engineering*, February 1980, Vol. 27, No. 2, and is reprinted in *MIC* with the permission of the authors and the publisher.

‡ Division of Automatic Control, SINTEF, NTH, N-7034 Trondheim, Norway.

§ 1977/78 on leave at the Department of Electrical Engineering and Computer Sciences, University of California, Berkeley, California 94720, U.S.A.

pulselength, wave diffraction) in such measurements, the Doppler signal from a range cell will be composed of a spectrum of frequencies. It is then interesting to know the response of phase estimators to such signals.

In this paper we derive the expected value of Doppler frequency estimators proposed for the use in MTI ultrasonic blood velocity measurements. We also give three new estimators. It is discussed how the expected values for the different estimators relate to the Doppler spectrum.

2. Formulation of the problem

Let a train of short ultrasonic pulses with angular r.f. frequency ω_0 and repetition frequency $f_s = 1/T_s$, be transmitted towards the blood vessel. $\omega_s = 2\pi f_s$ is the angular repetition frequency of the pulses. The received signal from the kth pulse may be written as (Angelsen 1980)

$$e_k(z) = \mathrm{Re}\,\{\hat{x}_k(z)\exp(i2k_0z)\} \tag{1}$$

where z is the depth of the range cell from which the signal is received and $k_0 = \omega_0/c$. c is the velocity of sound.

$$z = \tfrac{1}{2}ct \tag{2}$$

where t is the elapsed time between pulse transmission and echo arrival. The complex envelope $\hat{x}_k$ may be split into the in phase, x_k, and quadrature, y_k, components by

$$\hat{x}_k(z) = x_k(z) + iy_k(z) \tag{3}$$

We also note that we can write

$$e_k(z) = V_k(z)\cos[2k_0z + \phi_k(z)] \tag{4}$$

where

$$V_k = |\hat{x}_k| \quad \text{and} \quad \phi_k = \angle\hat{x}_k \tag{5}$$

$\hat{x}_k(z)$ with z as a fixed depth parameter can be considered as samples of the continuous Doppler signal $\hat{x}_t(z)$ from the range cell at depth z. We consider time invariant velocity fields. $\hat{x}_t$ can be obtained as the integral of uncorrelated contributions over the volume of scatterers. It is, therefore, a zero mean stationary gaussian process (Angelsen 1980). Thus all available information in $\hat{x}$ about the velocity field is contained in the power spectrum $G_{\hat{x}\hat{x}}(\omega, z)$ of $\hat{x}$ or its autocorrelation function $R_{\hat{x}\hat{x}}(\tau, z)$. In the following we shall omit z from our formulas where this is not confusing, assuming that we are studying the signal for a fixed depth z. We then have

$$R_{\hat{x}\hat{x}}(\tau) = 2(R_{xx}(\tau) + iR_{xy}(\tau)) \tag{6}$$

where the correlation function $R_{pq}(\tau)$ is defined as

$$R_{pq}(\tau) = \langle p^*(t)q(t+\tau)\rangle$$

* denotes complex conjugation and $\langle(\cdot)\rangle$ denotes ensemble expectation. We have used that $R_{yy} = R_{xx}$ and $R_{yx} = -R_{xy}$ for e_k to be stationary.

The power spectrum of $\hat{x}_t$ is given by the Fourier transform of $R_{\hat{x}\hat{x}}$, i.e.

$$G_{\hat{x}\hat{x}}(\omega) = \int_{-\infty}^{\infty} d\tau\, R_{\hat{x}\hat{x}}(\tau)\exp(-i\omega\tau)$$

which gives

$$\left.\begin{aligned} G_{\hat{x}\hat{x}}(\omega) &= 2\{G_{xx}(\omega)+iG_{xy}(\omega)\} \\ G_{xx}(\omega) &= \tfrac{1}{4}\{G_{\hat{x}\hat{x}}(\omega)+G_{\hat{x}\hat{x}}(-\omega)\} \\ G_{xy}(\omega) &= \frac{1}{4i}\{G_{\hat{x}\hat{x}}(\omega)-G_{\hat{x}\hat{x}}(-\omega)\} \end{aligned}\right\} \tag{7}$$

R_{xx} is an even, while R_{xy} is an odd, function in τ. This is equivalent to $G_{xx}(-\omega)=G_{xx}(\omega)$, while $G_{xy}(-\omega)=-G_{xy}(\omega)$ which is obtained from eqn. (7). These properties will be used in the following.

In many cases $G_{\hat{x}\hat{x}}$ is so narrow-band that it can be represented by a single frequency; e.g. the mean frequency given by

$$\bar{\omega}=\frac{\int_{-\infty}^{\infty} d\omega\, \omega G_{\hat{x}\hat{x}}(\omega)}{\int_{-\infty}^{\infty} d\omega\, G_{\hat{x}\hat{x}}(\omega)}=\frac{1}{i}\frac{\dot{R}_{\hat{x}\hat{x}}(0)}{R_{\hat{x}\hat{x}}(0)}=\frac{\dot{R}_{xy}(0)}{R_{xx}(0)} \tag{8}$$

where the last equality is obtained from the even and odd properties of R_{xx} and R_{xy} respectively. The instrumentation for single frequency estimators is much simpler than complete spectral estimation and has therefore been used so far (Grandchamp 1975, Brandestini 1976, 1977).

In the following section we shall derive expectation values for proposed estimators and discuss how they relate to $\bar{\omega}$. Three new estimators are also given.

3. Survey of single frequency estimators

3.1. *High frequency storage*

We here discuss two estimators which work directly on the received echoes and thus require storage of the signal at high frequencies (1–10 MHz). In the following the echoes from tissue are considered to have been removed. The first estimator to be discussed has been proposed by Grandchamp (1975). The structure of the estimator is given in Fig. 1. The Hilbert transform $\hat{e}_k$ of e_k is given by

$$\hat{e}_k=\mathrm{Im}\,\{\hat{x}_k \exp(i2k_0z)\} \tag{9}$$

Fact 1

The expected value of the estimator given in Fig. 1 is

$$\omega_1=\frac{1}{T_s}\sin^{-1}\frac{R_{xy}(T_s)}{R_{xx}(0)} \tag{10}$$

Proof

If x and y are two zero mean gaussian variables, the following relation, which was first obtained by Van Vleck, holds (Papoulis 1965)

$$\langle \mathrm{sgn}\, x\, \mathrm{sgn}\, y\rangle=\frac{2}{\pi}\sin^{-1}\rho \tag{11}$$

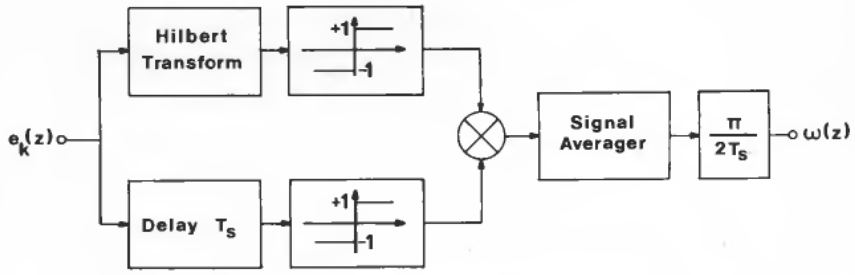

Figure 1. Doppler frequency estimator proposed by Grandchamp (1975).

where

$$\rho=\frac{\langle xy\rangle}{\sqrt{(\langle x^2\rangle\langle y^2\rangle)}}$$

and

$$\operatorname{sgn} x=\begin{cases}1 & x>0\\ -1 & x<0\end{cases}$$

Using this result we obtain

$$\omega_1=\frac{\pi}{2T_s}\langle \operatorname{sgn}\hat{e}_k \operatorname{sgn} e_{k-1}\rangle=\frac{1}{T_s}\sin^{-1}\frac{\langle \hat{e}_k e_{k-1}\rangle}{\langle e_k^2\rangle}$$

since stationarity implies $\langle e_{k-1}^2\rangle=\langle e_k^2\rangle$.

Now from eqns. (1) and (9) we obtain

$$\langle \hat{e}_k(z)e_{k-1}(z)\rangle=\frac{1}{4i}\langle[\hat{x}_k\exp(i2k_0z)-\hat{x}_k^*\exp(-i2k_0z)][\hat{x}_{k-1}\exp(i2k_0z)+\hat{x}_{k-1}^*\exp(-i2k_0z)]\rangle$$

$$=\frac{1}{4i}\{\langle\hat{x}_{k-1}\hat{x}_k\rangle\exp(i4k_0z)-\langle\hat{x}_{k-1}\hat{x}_k^*\rangle+\langle\hat{x}_{k-1}^*\hat{x}_k\rangle-\langle\hat{x}_{k-1}^*\hat{x}_k^*\rangle\exp(-i4k_0z)\}$$

By using eqn. (6) and the fact that $R_{xx}=R_{yy}$ are even functions while $R_{xy}=-R_{yx}$ are odd, we can show by straightforward calculation that

$$\langle\hat{x}_{k-1}\hat{x}_k\rangle=\langle\hat{x}_{k-1}^*\hat{x}_k^*\rangle=0$$

$$\langle\hat{x}_{k-1}^*\hat{x}_k\rangle=R_{\hat{x}\hat{x}}(T_s)$$

$$\langle\hat{x}_{k-1}\hat{x}_k^*\rangle=R_{\hat{x}\hat{x}}^*(T_s)$$

From this we obtain

$$\langle\hat{e}_k e_{k-1}\rangle=R_{xy}(T_s)$$

In the same way we show that $\langle e_k^2\rangle=R_{xx}(0)$ and the proof is completed.

$V_k(z)$ in eqn. (4) is low-pass and $\geqslant 0$. Thus by far most of the zero crossings of $e_k(z)$ are given by the cos term in eqn. (4). The phase change $\Delta_k=\phi_k-\phi_{k-1}$ can then be obtained from the zero crossings of the $e_k(z)$ and $e_{k-1}(z)$. Let z_1 be defined by

$$2k_0z_1+\phi_{k-1}(z_1)=\pi/2 \tag{12}$$

Then z_1 is a zero for $e_{k-1}(z)$. For the echoes from the following pulse, $e_k(z)$, this zero has moved to z_2 since ϕ_t has changed

$$2k_0 z_2 + \phi_k(z_2) = \pi/2 \tag{13}$$

From these two equations

$$\phi_k(z_2) - \phi_{k-1}(z_1) = 2k_0(z_1 - z_2) \tag{14}$$

z_1 and z_2 are so close that due to the low-pass nature of ϕ_t, we have $\phi_k(z_2) \approx \phi_k(z_1)$.

Brandestini (1976) has proposed an estimator which uses the zero crossings of $e_k(z)$ and $e_{k-1}(z)$ to estimate Δ_k in a way basically given by eqn. (14). However, due to the periodicity of cos x, $|\Delta_k| > \pi$ will be mapped into the region $[-\pi, \pi]$ by adding or subtracting multiples of 2π. This is demonstrated by the M function in Fig. 3. The expected value of the estimator will then be

$$\omega_2 = \frac{1}{T_s} \langle M(\Delta_k) \rangle \tag{15}$$

The structure of this estimator is given in Fig. 2. The phase detection is performed by the use of two D-type flip-flops.

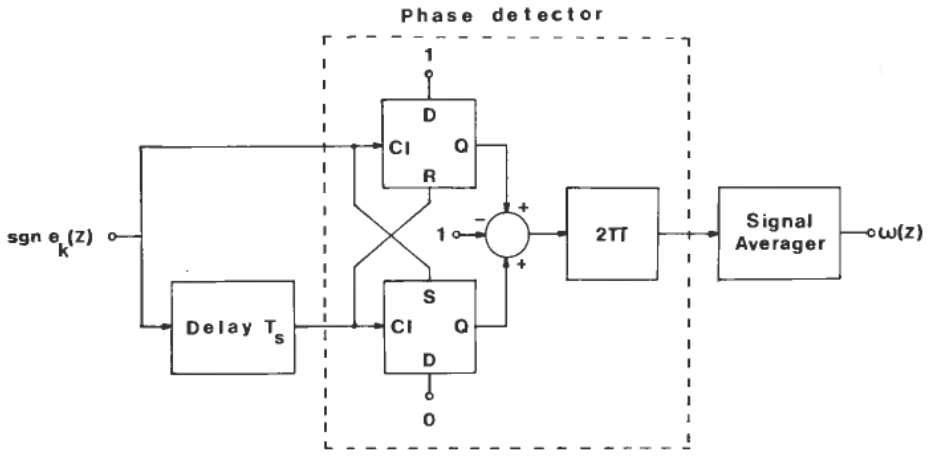

Figure 2. Estimator proposed by Brandestini (1976, 1977).

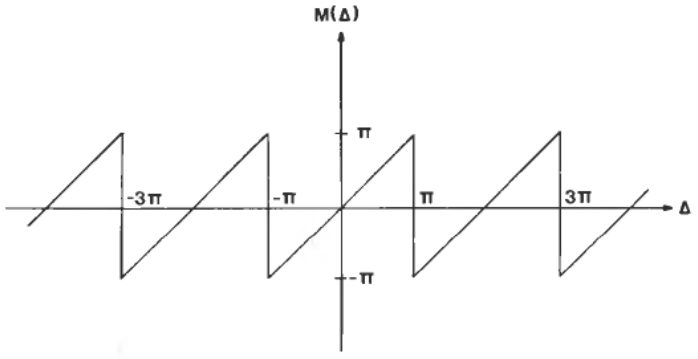

Figure 3. Mapping function of the phase detector shown in Fig. 2.

Fact 2

The estimator in Fig. 2 has the following expected value

$$\omega_2=\frac{1}{T_s}\psi-\omega_s A_0 \operatorname{sgn}\psi \tag{16}$$

$$\psi=\angle R_{\hat{x}\hat{x}}(T_s)$$

A_0 is given in eqn. (21).

Proof

Since stationarity is assumed, we obtain

$$\langle M(\Delta_k)\rangle=\langle M(\phi_2)\,|\,\phi_1=0\rangle \tag{17}$$

Now, by Bayes rule

$$p_{\phi_2|\phi_1}(\phi_2\,|\,\phi_1)=\frac{p_{\phi_1,\phi_2}(\phi_1,\phi_2)}{p_{\phi_1}(\phi_1)}$$

From the expressions of p_{ϕ_1} and $p_{\phi_1\phi_2}$ given in Davenport and Root (1958, p. 161, eqn. (8.92) and p. 164, eqn. (8.106)), we obtain

$$p_{\phi_2|\phi_1}(\phi_2\,|\,0)=\begin{cases} f(\phi_2-\psi) & \phi_2\in[-\pi,\pi] \\ 0 & \text{otherwise} \end{cases} \tag{18}$$

where

$$\psi=\angle R_{\hat{x}\hat{x}}(T_s)$$

and

$$\left.\begin{aligned} f(x)&=\frac{\Lambda^{1/2}}{2}\,\frac{\sqrt{(1-\alpha^2)}-\alpha\cos^{-1}\alpha}{(1-\alpha^2)^{3/2}} \\ \alpha&=-[\rho_{xx}^2(T_s)+\rho_{xy}^2(T_s)]^{1/2}\cos x \\ \Lambda^{1/2}&=1-\rho_{xx}^2(T_s)-\rho_{xy}^2(T_s) \\ \rho_{xx}(T_s)&=R_{xx}(T_s)/R_{xx}(0),\quad \rho_{xy}(T_s)=R_{xy}(T_s)/R_{xx}(0) \end{aligned}\right\} \tag{19}$$

We note that $f(-x)=f(x+2\pi)=f(x)$, i.e. f is periodic with period 2π. A typical plot of f is shown in Fig. 4.

The probability density above is defined for $\phi_2\in[-\pi,\pi]$. ϕ_t is the argument of the phasor $\hat{x}_t$, and when we follow $\hat{x}_t$ continuously, values of ϕ_t outside this region occur. These values should be mapped into $[-\pi,\pi]$ by adding multiples of 2π. This is the same mapping as shown in Fig. 3. By the way ϕ_2 enters into eqn. (18) we see that the M-mapping is automatically taken care of.

We are now in a position to calculate

$$\langle M(\phi_2)\,|\,\phi_1=0\rangle=\int_{-\pi}^{\pi} d\phi_2\,\phi_2 f(\phi_2-\psi)$$

$$=\psi+\int_{-\pi-\psi}^{\pi-\psi} dx\,x f(x)$$

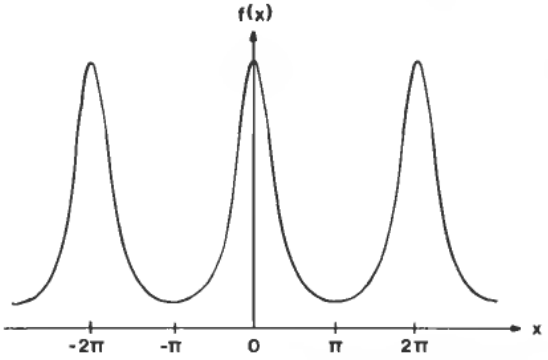

Figure 4. Typical plot of the conditional phase angle probability density function $f(x)$.

By straightforward manipulation and taking into account the periodicity of f we obtain

$$\langle M(\phi_2)|\phi_1=0\rangle=\psi-2\pi A_0 \operatorname{sgn}\psi \tag{20}$$

$$A_0=\int_{\pi-|\psi|}^{\pi} dx\, f(x) \tag{21}$$

This completes the proof.

Comment

The last term in eqns. (16) and (20) arises from the ambiguity of the zero crossings of the process e_k. If $\Delta_k=\pi+\delta$ then it is mapped onto $-\pi+\delta$ by subtracting -2π. This is accounted for by this last term.

3.2. *Low-pass storage*

The above two estimators work on the r.f. signal and therefore require storage of high frequency signals. In order to use digital storage or analogue storage in charge transfer devices it would be desirable to work directly on the information process $\hat{x}_k(z)$, which is low-pass.

Brandestini (1977) has proposed to use a time discrete zero crosser (TDZC) by using the average number of polarity changes per unit time of $x_k(z)$ (as a function of k for fixed z), for the discrete changes of interest. For a single frequency signal this estimator evidently works well when $\omega<\omega_s/2$. It is, however, non-directive (i.e. it does not give the sign of the Doppler shift) which to some extent may be overcome by certain tricks (Brandestini 1977).

The expected value of the TDZC may be described by the following equation:

$$\omega_3=\frac{\pi}{2T_s}\langle|\operatorname{sgn} x_k-\operatorname{sgn} x_{k-1}|\rangle \tag{22}$$

Let N_T be the number of zero crossings of a process x_t during the time interval T. Then it is known that (Papoulis 1965)

$$\frac{1}{T}\langle N_T\rangle=\frac{1}{\pi}\left\{\frac{\int_{-\infty}^{\infty} d\omega\,\omega^2 G_{xx}(\omega)}{\int_{-\infty}^{\infty} d\omega\, G_{xx}(\omega)}\right\}^{1/2}=\frac{1}{\pi}\left(-\frac{\ddot{R}_{xx}(0)}{R_{xx}(0)}\right)^{1/2} \tag{23}$$

i.e. twice the r.m.s. average frequency of the spectrum. For the TDZC the following result holds.

Fact 3

The TDZC has the following expected value

$$\omega_3 = \frac{1}{T_s} \cos^{-1} \frac{R_{xx}(T_s)}{R_{xx}(0)} \tag{24}$$

Proof

$$\langle |\operatorname{sgn} x_k - \operatorname{sgn} x_{k-1}| \rangle = \langle |\operatorname{sgn} x_2 - \operatorname{sgn} x_1| \rangle$$

$$= 2 \int_{-\infty}^{0} dx_1 \int_{0}^{\infty} dx_2 \, p_{x_1 x_2}(x_1, x_2) + 2 \int_{0}^{\infty} dx_1 \int_{-\infty}^{0} dx_2 p_{x_1 x_2}(x_1, x_2)$$

$$= 4 \int_{0}^{\infty} dx_1 \int_{0}^{\infty} dx_2 \, p_{x_1 x_2}(-x_1, x_2)$$

Then by direct calculation for gaussian variables which is given in the Appendix, we obtain

$$\langle |\operatorname{sgn} x_2 - \operatorname{sgn} x_1| \rangle = \frac{2}{\pi} \cos^{-1} \frac{R_{xx}(T_s)}{R_{xx}(0)}$$

and eqn. (24) is proved.

Comment

The TDZC gives a different expected value than the continuous zero crosser. The reason for this is that for signals with non-zero bandwidth there is a non-zero probability that there is more than one zero crossing between two adjacent samples. This occurs although the sampling frequency is greater than twice the maximum frequency of the signal which is the requirement for complete reconstruction of the signal. For a signal with non-zero bandwidth the TDZC will give an output which is less than the angular r.m.s. frequency of the signal.

An estimator which gives the same expected value as the TDZC can be obtained from the following equation

$$\omega_4 = \frac{1}{T_s} \sin^{-1} \frac{\langle |x_k - x_{k-1}| \rangle}{2 \langle |x_k| \rangle} \tag{25}$$

This estimator utilizes the normalized beat amplitude between the direct and the delayed signal. For practical estimators the ensemble expectations in eqns. (22) and (25) are obtained as time averages.

Fact 4

The expectation value of the beat amplitude estimator given in eqn (25) is the same as for the TDZC.

Proof

Assuming zero mean gaussian variables, we have

$$\langle |x_{k-1} - x_k| \rangle = \sqrt{\left[\frac{2}{\pi} \langle (x_{k-1} - x_k)^2 \rangle \right]} = \sqrt{\left[\frac{4}{\pi} (R_{xx}(0) - R_{xx}(T_s)) \right]}$$

$$\langle |x_{k-1}| \rangle = \sqrt{\left(\frac{2}{\pi} \langle x_{k-1}^2 \rangle \right)} = \sqrt{\left(\frac{2}{\pi} R_{xx}(0) \right)}$$

From this we obtain

$$\omega_4=\frac{1}{T_s}\sin^{-1}\sqrt{\left[\frac{1-\rho_{xx}(T_s)}{2}\right]}=\frac{1}{T_s}\cos^{-1}\rho_{xx}(T_s)$$

which completes the proof.

An estimator operating on $\hat{x}_k$ can be based on the following approximation to eqn. (8) ($R_{xy}(0)=0$):

$$\frac{\dot{R}_{xy}(0)}{R_{xx}(0)}\approx\frac{1}{T_s}\frac{R_{xy}(T_s)}{R_{xx}(0)}=\frac{1}{T_s}\frac{R_{\mathrm{sgn}\,x\,y}(T_s)}{R_{y\,\mathrm{sgn}\,y}(0)} \tag{26}$$

The last equality follows from Bussgangs relation which states that for two zero mean gaussian variables x and y (Papoulis 1965)

$$\langle y\,\mathrm{sgn}\,x\rangle=\sqrt{\left(\frac{2}{\pi}\right)}\frac{\langle xy\rangle}{\sqrt{\langle x^2\rangle}} \tag{27}$$

If $\hat{x}_t=\exp(i\omega t)$, i.e. a single frequency signal, we obtain

$$\frac{1}{T_s}\frac{R_{xy}(T_s)}{R_{xx}(0)}=\frac{1}{T_s}\sin\omega T_s$$

This indicates that the following expression should be a more useful basis for an estimator

$$\omega_5=\frac{1}{T_s}\sin^{-1}\frac{\langle x_{k-1}y_k\rangle}{\langle y_k{}^2\rangle}=\frac{1}{T_s}\sin^{-1}\frac{\langle y_k\,\mathrm{sgn}\,x_{k-1}\rangle}{\langle|y_k|\rangle} \tag{28}$$

For a single frequency signal with $\omega<\omega_s/4$ we then have $\omega_5=\omega$. We also note that this is the same expression as that given in eqn. (10), and this estimator therefore gives the same result as estimator 1.

From the $\sin^{-1}$ law of gaussian variables, eqn. (11), we also note that the following expression can be used as a basis for an estimator

$$\omega_6=\frac{\pi}{2T_s}\langle\mathrm{sgn}\,x_{k-1}\,\mathrm{sgn}\,y_k\rangle=\frac{1}{T_s}\sin^{-1}\frac{R_{xy}(T_s)}{R_{xx}(0)} \tag{29}$$

From eqn. (11) we also obtain the following result (Pawula 1968)

$$\left\langle\mathrm{sgn}\,x(t)\left[\frac{d}{dt}\mathrm{sgn}\,y(t)\right]\right\rangle=\frac{2}{\pi}\frac{\dot{R}_{xy}(0)}{R_{xx}(0)}=\frac{2}{\pi}\bar{\omega} \tag{30}$$

which suggests an estimator based on the following equation

$$\omega_7=\frac{\pi}{2T_s}\langle[\mathrm{sgn}\,y_k-\mathrm{sgn}\,y_{k-1}]\,\mathrm{sgn}\,x_{k-1}\rangle \tag{31}$$

Since $R_{xy}(0)=0$, $\omega_6=\omega_7$, but the formula in eqn. (31) suggests a different realization than that in eqn. (29). In order to minimize the amount of storage required, it is convenient to replace the term $\mathrm{sgn}\,x_{k-1}$ with $\mathrm{sgn}\,x_k$ in eqn. (31). This operation only results in a change of sign in the expectation value.

In view of Figs. 1 and 2 a realization of these last five estimators should be evident.

4. Discussion and examples

The estimators 1, 5, 6, and 7 give identical results while estimators 2, 3, and 4 differ from the rest of the group. Although the formulas are identical, the basic expressions, eqns. (10), (28), (29) and (31) suggest different implementations. Estimator 2 requires storage of the r.f. signal while estimator 1 only requires storage of samples of the r.f. signal (1–10 MHz) for estimation at discrete depths. The rest of the estimators require storage of a low-pass signal (< 300 kHz). For all estimators it is required to store the sign of the signal only, which may be performed by a 1 bit digital shift register. However, when the r.f. signal is stored, this requires a large number of bits in the register, which emphasizes analogue storage in this case (acoustic delay line). All estimators require storage of one echo only. Estimators 4 and 5 require a division to normalize for signal amplitude.

All estimators, except 3 and 4, are directional, i.e. the polarity of the output give the sign of the Doppler shift. For a single frequency Doppler signal all estimators give an unbiased estimate, provided its frequency is below a limit. This limit is $\omega_s/2$ for estimators 2, 3 and 4, while it is $\omega_s/4$ for estimators 1, 5, 6 and 7. The estimator outputs for a single frequency signal are shown in Fig. 5.

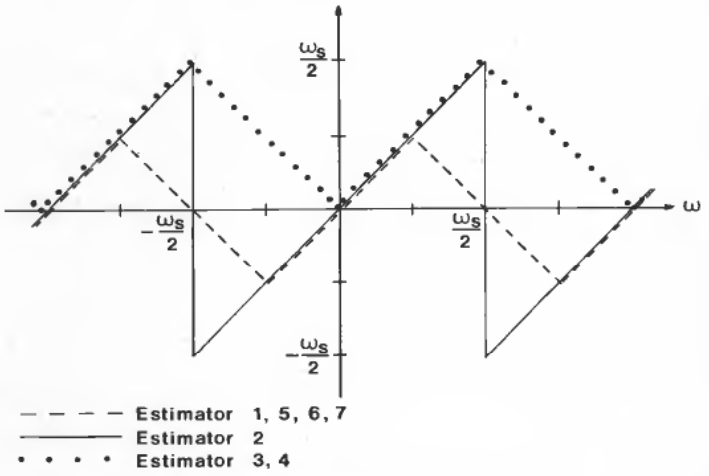

Figure 5. Estimator outputs for single frequency Doppler signal output.

For the case of non-zero signal bandwidth we study the following spectrum which is indicated in Fig. 6:

$$G_{\hat{x}\hat{x}}(\omega) = G(\omega - \bar{\omega}) \tag{32}$$

where $\bar{\omega}$ is the mean angular frequency of $G_{\hat{x}\hat{x}}$ defined in eqn. (8) and $G(\omega)$ is low-pass.

The autocorrelation function of $\hat{x}$ will be

$$R_{\hat{x}\hat{x}}(\tau) = \exp(i\omega t)\hat{R}(\tau) \tag{33}$$

where $\hat{R}(\tau) = R_e(\tau) + iR_o(\tau)$ is the inverse Fourier transform of $G(\omega)$. The subscripts e and o, indicate that the functions are even and odd respectively. From eqns. (6)

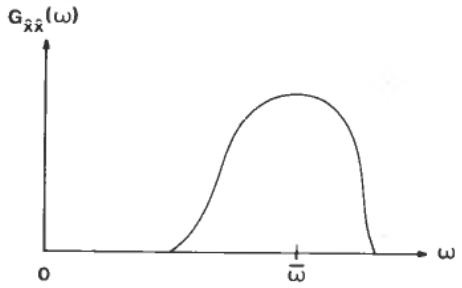

Figure 6. Typical power spectrum of the Doppler signal.

and (33) we obtain

$$\left.\begin{aligned} R_{xx}(\tau) &= \tfrac{1}{2}R(\tau)\cos\left[\bar{\omega}\tau+\theta(\tau)\right] \\ R_{xy}(\tau) &= \tfrac{1}{2}R(\tau)\sin\left[\bar{\omega}\tau+\theta(\tau)\right] \end{aligned}\right\} \tag{34}$$

where $R=|\hat{R}|$ and $\theta=\angle\hat{R}$. The output of estimators 1, 5, 6 and 7 will, for this signal, be

$$\left.\begin{aligned} \omega_{1,5,6,7} &= \frac{1}{T_s}\sin^{-1}\{\rho(T_s)\sin\left[\bar{\omega}T_s+\theta(T_s)\right]\} \\ \rho(T_s) &= R(T_s)/R(0) \end{aligned}\right\} \tag{35}$$

Note that if $G(-\omega)=G(\omega)$, i.e. $G_{\hat{x}\hat{x}}(\omega)$ symmetric around $\bar{\omega}$, $R_0(\tau)\equiv 0$, which implies $\theta\equiv 0$.

If the bandwidth of $G(\omega)$ is small compared to ω_s, $\rho(T_s)\approx 1$ and $\theta(T_s)\approx 0$ so that we obtain

$$\omega_{1,5,6,7}\approx\bar{\omega}$$

For estimator 2 we obtain from eqn. (16) with the above signal spectrum

$$\omega_2=\bar{\omega}+\frac{1}{T_s}\theta(T_s)-\omega_s A_0\,\mathrm{sgn}\left[\bar{\omega}+\frac{1}{T_s}\theta(T_s)\right] \tag{36}$$

A_0 must be determined numerically. For a narrow-band signal $\theta\approx 0$ and $A_0\approx 0$ which give

$$\omega_2\approx\bar{\omega}$$

For estimators 3 and 4 we get the following output according to eqn. (24)

$$\omega_{3,4}=\frac{1}{T_s}\cos^{-1}\{\rho(T_s)\cos\left[\bar{\omega}T_s+\theta(T_s)\right]\} \tag{37}$$

Again we have as for the above estimators that when $\hat{x}$ is narrow-band

$$\omega_{3,4}\approx\bar{\omega}$$

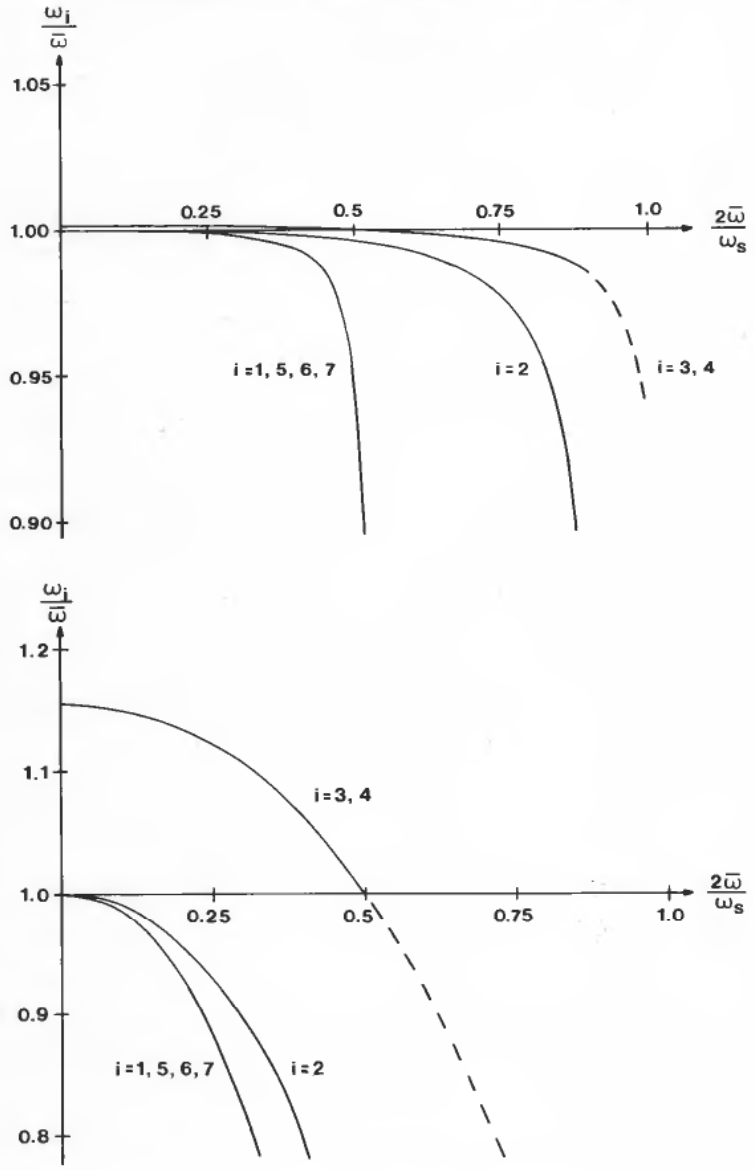

Figure 7. Expectation value of the estimators as a function of the mean angular frequency of the power spectrum, (*a*) $B=0{\cdot}2\bar{\omega}$; (*b*) $B=2\bar{\omega}$.

When $T_s \to 0$, the argument of $\cos^{-1}$ in eqn. (37) tends to 1 and $\cos^{-1} q \approx \sqrt{2(1-q)}$, $q \lesssim 1$, which give ($\dot{R}_{xx}(0)=0$):

$$\lim_{T_s \to 0} \omega_{3,\,4} = [-\ddot{R}_{xx}(0)/R_{xx}(0)]^{1/2} = \omega_{\text{r.m.s.}}$$

i.e. the same value as for the continuous zero crosser. The reason for this is that when $\bar{\omega}T_s$ becomes small, the probability of multiple zero crossings in an interval of length T_s tends towards zero.

To get an idea of the magnitude of the difference between the estimator outputs and the average Doppler frequency we perform numerical calculations for the

following spectrum:

$$G(\omega)=\begin{cases}\dfrac{4\pi}{B} & |\omega|<\dfrac{B}{2}\\ 0 & \text{otherwise}\end{cases} \tag{38}$$

with the following two bandwidths

$$B_1=0.2\bar{\omega}, \quad B_2=2\bar{\omega}$$

For this spectrum we obtain

$$R(\tau)=2\frac{\sin\dfrac{B\tau}{2}}{\dfrac{B\tau}{2}} \tag{39}$$

We note that since the spectrum is symmetric, $\theta=0$. The results for the different estimators are shown in Fig. 7.

In both cases the performance of estimator 2 is clearly superior to that of estimators 1, 5, 6 and 7. When $B=B_1$, the bias of estimator 2 is small as long as the maximum frequency ω_M of $G_{\hat{x}\hat{x}}(\omega)$ is less than the Nyquist frequency. In the broad-band case, however, the bias of ω_2 is quite large, even for ω_M well below $\omega_s/2$. The reason for this is easily understood from Fig. 8, which shows plots of $f(x)$ for two different bandwidths. It is apparent that $f(x)$ gets broader when B increases. When $\bar{\omega}$ is a constant, this results in a larger A_0 which accounts for the increasing bias of estimator 2 when the relative bandwidth $B/\bar{\omega}$ increases.

The bias of the non-directive estimators 3 and 4 is also negligible when $G_{\hat{x}\hat{x}}$ is narrow-band. When $B=B_2$ and $\bar{\omega}$ is small, this group overestimates with about 15%, but the bias decreases with increasing $\bar{\omega}$, passing through zero when $\bar{\omega}=\omega_0/4$. We see from eqn. (37) that this is valid invariant of B for $\theta=0$. Because of the non-directivity of these estimators, the error does not increase drastically as ω_M passes through $\omega_s/2$.

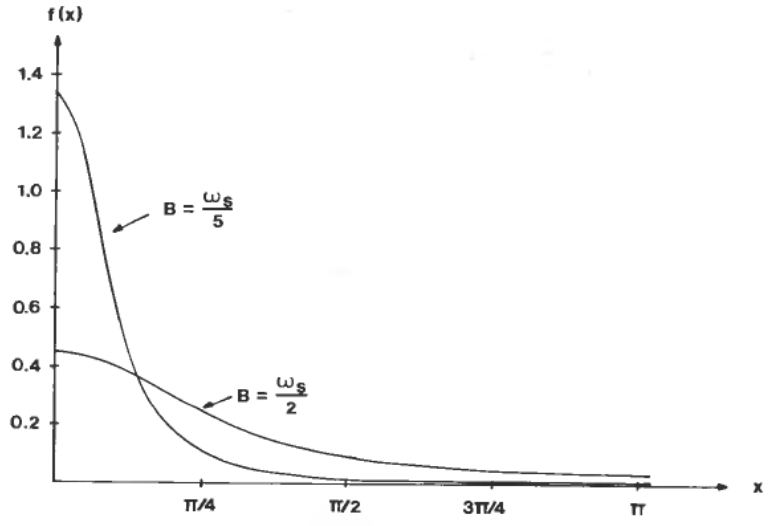

Figure 8. Dependence of $f(x)$ upon the bandwidth of the power spectrum.

Appendix

The second-order gaussian probability density is given by

$$p_{x_1x_2}(x_1, x_2)=\frac{1}{2\pi\sigma^2\sqrt{(1-\rho^2)}}\exp\left\{-\frac{x_1^2+x_2^2-2\rho x_1x_2}{2\sigma^2\sqrt{(1-\rho^2)}}\right\}$$

$$\sigma^2=R_{x_ix_i}(0)$$

$$\rho=R_{x_1x_2}(T_s)/R_{x_ix_i}(0), \quad i=1,2$$

We here give the details of the integration for the proof of eqn. (24). By changing variables of integration

$$x_1=r\cos\theta$$

$$x_2=r\sin\theta$$

we obtain

$$I=4\int_0^\infty dx_1\int_0^\infty dx_2\, p_{x_1x_2}(-x_1, x_2)$$

$$=\frac{2}{\pi\sigma^2\sqrt{(1-\rho^2)}}\int_0^\infty dr\, r\int_0^{\pi/2} d\theta\exp\left\{-r^2\frac{1+\rho\sin 2\theta}{2\sigma^2(1-\rho^2)}\right\}$$

$$=\frac{2\sqrt{(1-\rho^2)}}{\pi}\int_0^{\pi/2}\frac{d\theta}{1+\rho\sin 2\theta}$$

By substituting $z=\tan\theta$, we obtain

$$I=\frac{2}{\pi\sqrt{(1-\rho^2)}}\int_0^\infty\frac{dz}{1+\left[\dfrac{z+\rho}{\sqrt{(1-\rho^2)}}\right]}=\frac{2}{\pi}\tan^{-1}\left(\frac{z+\rho}{\sqrt{(1-\rho^2)}}\right)\Bigg|_0^\infty$$

$$I=\frac{2}{\pi}\left[\frac{\pi}{2}-\tan^{-1}\frac{\rho}{\sqrt{(1-\rho^2)}}\right]=\frac{2}{\pi}\cos^{-1}\rho$$

which completes the proof.

References

Angelsen, B. A. J. (1980). A Theoretical Study of the Scattering of Ultrasound from Blood. *I.E.E.E. Trans. Biomed. Engng*, **14**, pp. 61–67.

Brandestini, M. (1976). Signalverarbeitung in perkutanen Ultraschall Doppler Blutfluss Messgeräten. Thesis No. ETH 5711, Eindgenössischen Technischen Hochschule, Zürich; (1977). A transcutaneous *N*-channel digital Doppler. *Echocardiology with Doppler Application and Real Time Imaging*, edited by N. Bom (The Haag: Martinus Nijhoff Medical Division), pp. 357–368.

Davenport, W. B., Jr., and Root, W. L. (1958). *An Introduction to the Theory of Random Signals and Noise* (New York: McGraw-Hill).

Grandchamp, P. A. (1975). A novel pulsed directional Doppler velocimeter; the phase detection profilometer. *Proceedings of the 2nd European Congress on Ultrasonics in Medicine*, edited by: E. Kazner, M. de Vlieger, H. R. Müller and V. R. McCready (Amsterdam: Excerpta Medica), pp. 137–143.

Papoulis, A. (1965). *Probability, Random Variables and Stochastic Processes* (Tokyo: McGraw-Hill).

Pawula, R. F. (1968). Analysis of the Center Frequency of a Power Spectrum. *I.E.E.E. Trans. Inf. Theory*, **14**, pp. 669–675.

Skolnik, M. I. (1962). *Introduction to Radar Systems* (New York: McGraw-Hill), pp. 113–154.